Journal of Ship Research, Vol. 24, No. 3, Sept. 1980, pp. 135–146

Journal of
Ship Research

Leading-Edge Flutter of Supercavitating Hydrofoils

C. Brennen,[1] **K. T. Oey,**[1] and **C. D. Babcock**[1]

This paper presents the results of experiments and analysis of the phenomenon of leading-edge flutter which has been observed to occur for supercavitating hydrofoils. The experiments confirmed the existence of such a single-degree-of-freedom flutter involving chordwise bending and indicated that for long, natural (or vapor-filled) cavities the reduced flutter speed, $U_F/\omega_F c$, was in the range 0.15 to 0.23. Secondary effects observed were the variation with the angle of attack (a minimum flutter speed occurred at 10 deg) and with a foil mass ratio. Shorter cavities typically yielded lower flutter speeds due to a complex interaction between the bubble collapse process occurring in the cavity closure region and the unsteady hydrodynamic load on the foil. Finally, a relatively simple theoretical analysis for supercavitating hydrofoils with elastic axes aft of midchord is presented. This linear analysis yields reduced flutter velocities somewhat lower than those observed.

Introduction

HYDROFOILS utilized for hydrofoil boats, propeller blades, and pump or turbine blades are, of course, subject to the same kinds of fluid/structure interaction instabilities as airfoils [1].[2] However, increasing speeds led to the need to redesign foil shapes for efficient operation with large attached vapor- or gas-filled cavities; such redesigns involve relatively thin wedge-shaped foils with sharp and thin leading edges [2]. It has become apparent that such foils operating with fully developed cavities exhibit a hydroelastic instability which involves chordwise bending vibration of the thin leading edge. This phenomenon, which is termed "leading-edge flutter," is somewhat similar though not identical to airfoil stall flutter or leading-edge flap flutter in subsonic aeroelasticity. One of the earliest reported observations of leading-edge flutter was made in 1957 by Waid and Lindberg [3]. During performance tests of certain supercavitating foils in a water tunnel, they observed that at a certain critical speed the forward portion of the foil including the leading edge began to vibrate violently in a chordwise bending mode while the thick trailing-edge part of the foil remained relatively stationary (see Fig. 1). One result of this vibration was the creation of a train of waves on the cavity surface originating at the leading edge. Similar observations were made by Spangler [4]. There have also been reports of similar phenomena and failures in supercavitating propellers and inducer pumps.

These sketchy and early observations suggest (correctly as will be seen) that leading-edge flutter requires only a single elastic mode, namely, that of chordwise bending of the foil. This contrasts with conventional wing flutter, which involves two modes (usually spanwise bending and torsion, or, more fundamentally, pitching and heaving) interacting in such a way that the foil absorbs energy from the flow. Kaplan and Henry [5] and Song [6] have examined the conventional flutter potential for cavitating (or separated) flow theoretically and Song and Almo [7], Kaplan and Lehman [8], and others have performed conventional flutter experiments. Further discussion on these will be delayed until the final section.

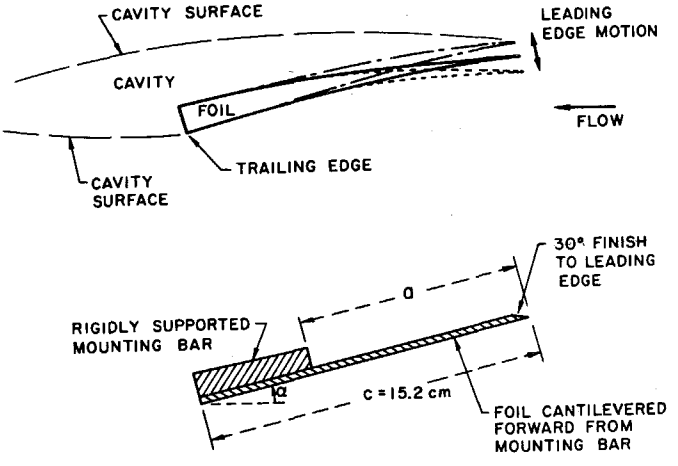

Fig. 1 *Above:* typical supercavitating hydrofoil shape with the leading-edge flutter mode and the cavity configuration sketched. *Below:* configuration of the models used in the experiments

One other phenomenon demands mention. It is well-known that hydrofoils with cavities extending from the leading edge to a length of between about ½ and 1½ chords (that is, closure in the neighborhood of the trailing edge) are unstable at almost any speed; the lift exhibits oscillations as the cavity oscillates between closure on the suction surface and a point downstream of the trailing edge. This will be referred to as partial cavitation instability; it is a purely fluid mechanical instability which can occur with a completely rigid foil. When the foil is flexible, however, the partial cavitation instability can lock into the natural structural frequency. In the context of the present study it will be seen that there is an overlap between leading-edge flutter and partial cavitation instability when the cavity length is short.

The present investigation was designed to concentrate primarily

[1] California Institute of Technology, Pasadena, California.

[2] Numbers in brackets designate References at end of paper.

Manuscript received at SNAME headquarters July 17, 1979; revised manuscript received September 20, 1979.

Table 1 Data on 15.2-cm-span foils

Foil No.	Thickness, t mm	Flexible/ Total Chord, a/c	Mass Ratio, $\mu^* = \rho_s t/\rho a$	First-Mode Frequency, Hz: In Air, $\omega_A/2\pi$	First-Mode Frequency, Hz: In "Still" Water, $\omega_W/2\pi$	Flutter Frequency, Hz, $\omega_F/2\pi$	Flutter Speeds for Long Cavities: U_F, m/s, $\alpha = 7°$	U_F, m/s, $\alpha = 10°$	U_F, m/s, $\alpha = 13°$	$U_F/\omega_F c$, $\alpha = 7°$	$U_F/\omega_F c$, $\alpha = 10°$	$U_F/\omega_F c$, $\alpha = 13°$
H31	0.787	0.583	0.024	71.6 (67.2)[a]	(8.9)[b]	[c]	...	...	...	...	...	...
H68	1.73	0.583	0.052	159.3 (147.4)[a]	51.2 (25.6)[b]	44	<11	...	...	<0.26	...	...
H89	2.26	0.583	0.069	195.7 (192.9)[a]	71.2 (42.5)[b]	60	11.6	8.5	9.8	0.20	0.15	0.17
H125	3.17	0.583	0.096	294.0 (270.4)[a]	95.8 (70.8)[b]	83	18.3	15.9	>18.3	0.23	0.20	>0.23
H50A	1.27	0.417	0.054	192.3 (212.4)[a]	56.0 (35.5)[b]	53	<8.9	...	...	<0.175	...	...
H125B	3.17	0.706	0.080	200.0 (185.5)[a]	80.1 (48.0)[b]	60	11.5 (8°)	10.9	12.3	0.20 (8°)	0.19	0.215

[a] Theoretical values using Barton's [14] method.
[b] Theoretical values using Lindholm et al's [15] method.
[c] Diverged and destroyed before a cavity could be formed.
NOTE: All foils have a chord of 15.2 cm.

on leading-edge flutter for long fully developed cavities and to minimize the complexities which might occur with the appearance of hybrid forms of instability such as that discussed in the preceding. The experimental observations will be described first; this will be followed by some theoretical considerations which help to explain the basic phenomenon.

Excitation systems and vibration characteristics of model foils

The foils tested were intended to model the gross structural features of supercavitating foils and yet be simple enough to be manufactured in significant number. As shown in Fig. 1, they consisted of thin flat aluminum plates (6061 T-6 aluminum) of various thicknesses; at the trailing edge they were bolted to a much thicker and stiffer mounting bar which essentially fixed the rear portion and trailing edge of the foils. All foils had a chord of 15.2 cm and their leading edges were machined with a 30-deg wedge to produce a clean, sharp cavity separation at this point. The length of the cantilevered flexible portion of the foil will be denoted by a and the total chord by c. The foils were each fitted with three strain gages bonded to the suction side of the flexible portion in order to monitor chordwise bending; the three gages were placed at midspan and near the ends of the span. One additional gage on the mounting bar registered the fluctuating lift (actually the force normal to the mounting bar). Dynamic calibrations were performed in air, using acoustic excitation in order to relate the output of the foil-mounted gages to the leading-edge displacement. The deflection mode shape under these conditions is close to that of the hydrodynamic mode under flowing conditions; any differences are neglected in Figs. 6 and 7. The mounting bar gage was calibrated statically.

Experiments were carried out in both the Free Surface Water Tunnel (FSWT) and the High Speed Water Tunnel (HSWT) in the Hydrodynamics Laboratory at the California Institute of Technology [9, 10]. The foils tested in these facilities had spans of 35.6 and 15.2 cm, respectively, and details are given in Tables 1 and 2. Most of the data presented here are taken from the more extensive series of tests conducted with natural or vapor-filled cavities in the HSWT, though some reference will be made to the tests with ventilated or air-filled cavities performed in the FSWT. Further detailed information can be found in Oey [11] and Brennen et al [12].

Most hydrofoils, propellers, or pump blades are supported in such a way that their modes of vibration are quite complicated; nodal lines do not lie simply in the chordwise or spanwise direction. Examples of mode shapes for a typical supercavitating hydrofoil are presented by Brennen et al [12] and for pump blades by Ost-

Nomenclature

a = flexible chord
c = chord
C_D = drag coefficient
C_M = coefficient of moment, $M/\frac{1}{2}\rho U^2 c^2$
E = modulus of elasticity
I = moment of inertia
I_0 = dimensionless moment of inertia, $I = I_0 \rho_s t c^2$
j = imaginary unit
k = reduced frequency, $\omega c/U$
l = cavity length
K = spring constant
M = hydrodynamic moment per unit span
p_∞ = freestream tunnel pressure
p_c = cavity pressure
Q = Q-factor, $\omega_N/\Delta\omega$
R = equivalent cylindrical radius of the pinched-off cavity
s = foil span
t = flexible foil thickness
T = time
U = tunnel velocity
U_D = tunnel velocity for foil divergence
y = leading-edge displacement
α = angle of attack
β = distance of hinge from leading edge/c
δ = leading-edge displacement amplitude
λ = wavelength of waves on leading-edge cavity surface
μ = mass ratio, $\rho_s t/\rho c$
μ^* = modified mass ratio, $\rho_s t/\rho a$
ν = kinematic viscosity of liquid
ρ = liquid density
ρ_s = foil material density
σ = cavitation number, $(p_\infty - p_c)/\frac{1}{2}\rho U^2$
ω = radian frequency
ω_{NV} = first-mode natural frequency of foil in vacuo
ω_A = first-mode natural frequency of foil in air
ω_W = first-mode natural frequency in "still" water
ω_N = first-mode natural frequence with flow
$\Delta\omega$ = half power bandwidth

Modifiers

subscript 0 refers to mean quantities
subscript R refers to real part
subscript I refers to imaginary part
subscript F refers to quantities at critical flutter conditions
tilde (~) over character refers to complex fluctuating quantity
dot (˙) over character denotes time derivative

Table 2 Data on 35.6-cm-span foils

Foil No.	Thickness, t, mm	Mass Ratio $\mu^* = \rho_s t/\rho a$	First-Mode Frequency, Hz: In Air $\omega_A/2\pi$	First-Mode Frequency, Hz: In "Still" Water $\omega_W/2\pi$	Second-Mode Frequency, Hz: In Air $\omega_A/2\pi$	Second-Mode Frequency, Hz: In "Still" Water $\omega_W/2\pi$	Divergence Speed	Flutter Frequency, Hz, $\omega_F/2\pi$	Flutter Speed, U_F	$U_F/\omega_F c$
F16	0.406	0.012	37.0	6.3			1.2	[g]	[g]	[g]
			(35)[a]	(2.2)[b]	(42)[a]	(4.3)[b]	(1.16)[c] (1.62)[d]			
F31	0.787	0.024	69.0	14.0		19.2	2.1	12	<1.2[f]	<0.106
			(67)[a]	(5.9)[b]	(82)[a]	(11.5)[b]	(3.2)[c] (4.4)[d]			
F61	1.55	0.047		37.5		50.5	[e]	38	~4	0.109
			(132)[a]	(16.1)[b]	(160)[a]	(31)[b]	(8.9)[c] (12.0)[d]			
F89	2.26	0.069	230.4	62.5	267	89.0	[e]	65	~7	0.113
			(193)[a]	(28.2)[b]	(234)[a]	(55)[b]	(15.6)[c] (21.3)[d]			

[a] Theoretical values using Barton's [14] method.
[b] Theoretical values using Lindholm et al's [15] method.
[c] Nonseparated flow theoretical value [12].
[d] Cavitating or wake flow theoretical value [12].
[e] Velocity not attainable in present experiments.
[f] Unbounded flutter occurred at the lowest speed at which a cavity could be formed.
[g] Noncavitating divergence occurred before a cavity could be formed.
NOTE: All foils have an a/c ratio of 0.583 with a chord (c) = 15.2 cm.

erwalder and Sonsino [13]. However, the present foils were deliberately intended to have fairly simple modes of vibration in order to facilitate comparison with theory.

The first natural frequencies of the model foils in air were measured by tuned excitation using an acoustical loudspeaker; these are listed in Tables 1 and 2. The first mode involved pure chordwise bending in every case; the second mode was similar except that the phase of the bending varied over the span with the ends out of phase by 180 deg and a node at midspan. In Tables 1 and 2 comparison is made with theoretical values for the first natural frequency in a vacuum obtained using the method described by Barton [14]. The agreement is fairly good and the small differences are probably due to aerodynamic damping and added mass.

A different excitation system was developed for tests under water. This was used for bench testing in tanks of "still" water and the experiments in the FSWT. A music wire attached to the leading edge (usually near midspan) was connected to an electromagnetic shaker. A weak spring and a load cell were interposed in the wire. The spring allowed decoupling of the motion of the shaker and the foil. The purpose of the load cell was to monitor the force applied to the foil. Since frequency response spectra are most meaningful when the amplitude of the applied force is constant, a feedback system was installed which automatically adjusted the motion of the shaker to ensure a constant preset level of force as monitored by the load cell. Using this system, frequency response spectra of the foil displacement as monitored by the foil strain gages were obtained using relatively low sweep rates. The bandwidth, $\Delta\omega$, about the resonant or natural frequency ω_N indicated the amount of damping for a particular foil under the prevailing fluid conditions.

In the bench tests in air this excitation system yielded natural frequencies identical to those obtained by acoustical excitation. The natural frequencies measured in "still" water are listed in Tables 1 and 2. They are compared with theoretical values obtained using the unmodified strip theory of Lindholm et al [15], which incorporates estimates of the added mass of the water. The large discrepancies between theory and experiment are similar to the discrepancies recognized by Lindholm et al in comparison with their experiments; there would appear to be considerable difficulty involved in the accurate prediction of the "still" water natural frequencies for foils with span/chord ratios of one or greater. Some of the difficulty may be due to lack of validity of the strip theory, though viscous and eddy-shedding characteristics of the real flow may also play a role. The theoretical values are substantially lower than the actual, indicating that the amount of fluid contributing to the added mass is much less than that anticipated by the strip theory. Later it will be seen that the natural frequencies (and flutter frequencies) of foil vibration in a cavitating flow are quite close to those in "still" water.

Some measurements of the damping of the 35.6-cm-span foils were also made in "still" water. The principal conclusion of this investigation as reported in Brennen et al [12] was that the damping was nonlinear and dependent on the oscillatory Reynolds number associated with the vibration. These measurements are only of incidental interest since the damping is quite dependent on viscous and eddy-shedding effects at the leading edge and these effects would probably be significantly different in the presence of an oncoming stream.

High-speed water tunnel experiments with natural cavities

The 15.2-cm-span foils were tested with natural vapor-filled cavities in the HSWT. The mounting system is shown in Fig. 2. The independent velocity and pressure regulation in this tunnel allowed observations of flutter onset for a wide range of foil thicknesses (see Table 1) over a wide range of speeds (4.5 to 18.5 m/s), angles of attack (7 to 13 deg), and cavitation numbers (from short to long cavities).

When the tunnel velocity was raised for a given cavity length, the onset of leading-edge flutter in these HSWT tests was sudden, dramatic, and repeatable. It not only could be recognized by the sudden appearance of a sinusoidal output from the strain gages but was also visible and audible. Furthermore, the appearance of the cavity would change as illustrated by Fig. 3 and discussed later.

The flutter speed for a given foil at a particular angle of attack tended to a maximum asymptotic value for long cavities (shown later). These long cavity flutter speeds ranged from 8.5 to 19.8 m/s for Foils H68, H89, H125, H50A, and H125B (Foil H31 diverged and was destroyed before a cavity could be formed). However, when the flutter speeds, U_F, were nondimensionalized using the flutter frequency, ω_F (see Table 1), the resulting values all lay between 0.15 and 0.23 as illustrated in Fig. 4. The arrows in this figure indicate that the flutter speeds for H68 and H50A at $\alpha = 7$ deg had not reached a clear limit for the longest cavity conditions examined; also, the flutter speed for H125 at $\alpha = 13$ deg seemed to be a little above the maximum velocity of the tunnel under these conditions.

An angle of attack of about 10 deg consistently manifests the lowest flutter speed (see Fig. 4). The reason for this is not clear. It should also be recorded that a few spot-checks at negative angles

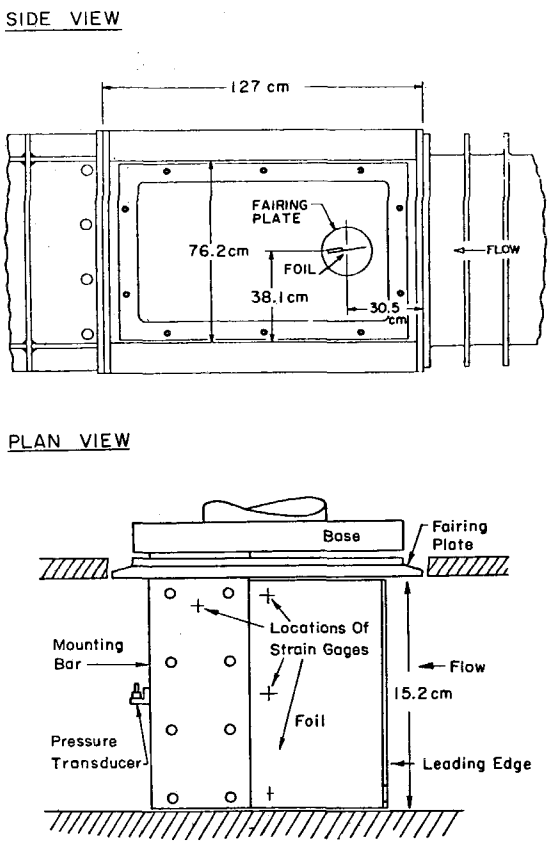

Fig. 2 Mounting system for the 0.152-m-span foils in the High Speed Water Tunnel

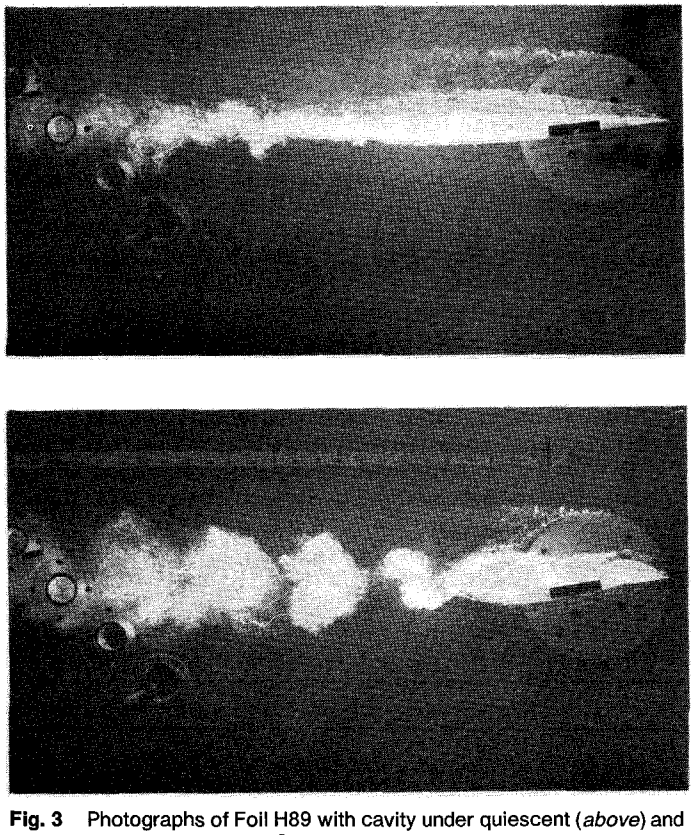

Fig. 3 Photographs of Foil H89 with cavity under quiescent (*above*) and fluttering (*below*) conditions [α = 7 deg (*above*) and 10 deg (*below*); velocity = 6.6 m/s (*above*) and 7.4 m/s (*below*)]

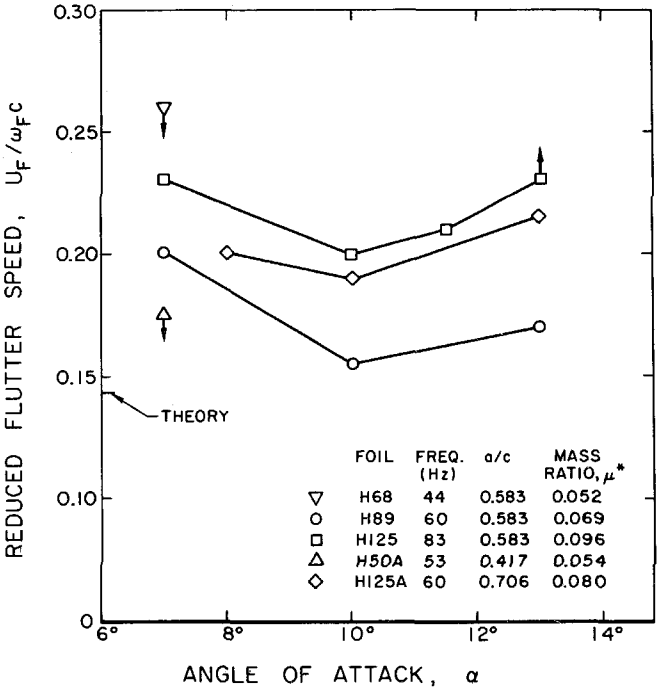

Fig. 4 Reduced flutter speeds, $U_F/\omega_F c$, for long cavities as a function of angle of attack. The theoretical value of 0.143 is indicated on the vertical axis

of attack with the mounting system inverted indicated flutter speeds and flow patterns identical to those at a positive angle of attack. This eliminated the possibility of any Froude number or buoyancy effect in the phenomenon.

The values of $U_F/\omega_F c$ for different foils with long cavities seem to be displaced up or down in Fig. 4 by the same amount at all angles of attack. Leaving aside for the moment the dependence on cavitation number (or cavity length to chord ratio), one would expect parametrically that the reduced flutter speeds for these geometrically similar foils should depend only on α, the mass ratio $\mu = \rho_s t/\rho c$, and the flexible-chord/total-chord ratio, a/c. Collation of the data in Fig. 4 with the tabulated values of a/c and a modified mass ratio, $\mu^* = \rho_s t/\rho a$, included in that figure suggests a fairly consistent increase in the reduced flutter speed with increasing μ^* and no consistent separate trend with a/c.

The effect of cavity length (or cavitation number) on the flutter speed was similar for all foils and is typified by the results presented in Fig. 5. For angles of attack of 10 deg and above, there was only a very slight decrease in the flutter speed as the cavity length was decreased. At lengths less than about 2 chords the amplitude would increase markedly as the leading-edge flutter phenomenon began to merge with the partial cavitation instability (see Figs. 6 and 7). The danger of foil and tunnel damage limited the experiments that could be performed in this short cavity regime.

Cavity length had a more marked effect on the flutter speed at the smaller angles of attack (7 and 8 deg) as indicated in Fig. 5. In addition to the decrease in flutter speed with decreasing length, a rather interesting "resonant length" phenomenon occurred. The experiments were often carried out by setting the tunnel speed at a value just a little less than the long cavity flutter speed and subsequently decreasing the cavity length by increasing the tunnel pressure. At the low angles of attack, flutter would occur at some cavity length but subsequently disappear as the length was decreased, only to appear again at another resonant length. These "resonant lengths" were often integer multiples of the chord length. This accounts for the hatched area in Fig. 5 where all the onset points are plotted. This effect probably represents one in-

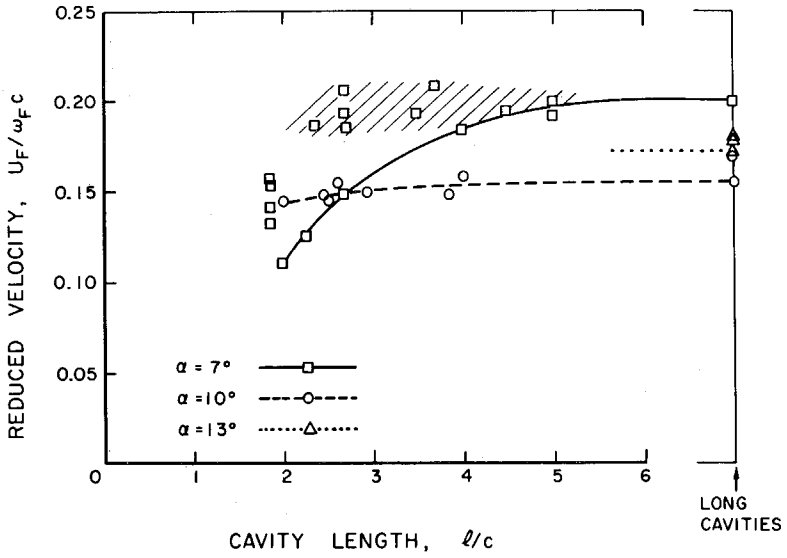

Fig. 5 Flutter speed and boundaries as a function of cavity length for Foil H89 at $\alpha = 7$, 10, and 13 deg. Values on the extreme right are for cavities which extended beyond the extent of the window in the working section. The hatched area and the points in it represent the regime of the resonant-length phenomenon

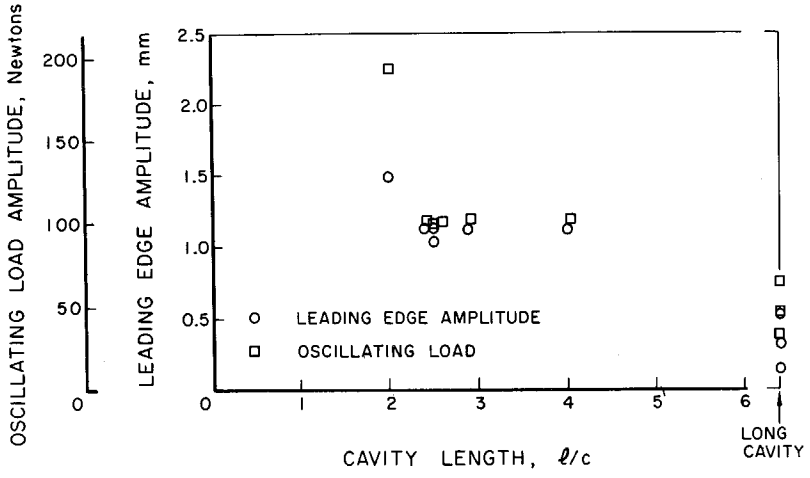

Fig. 6 Leading-edge amplitude and oscillating load versus cavity length for Foil H89 at an angle of attack of 10 deg

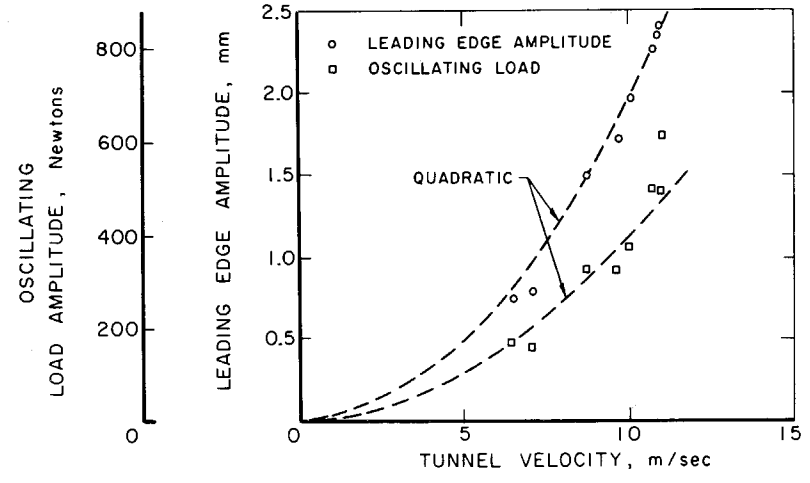

Fig. 7 Leading-edge amplitude and oscillating load versus flutter velocity for Foil H89 at an angle of attack of 7 deg

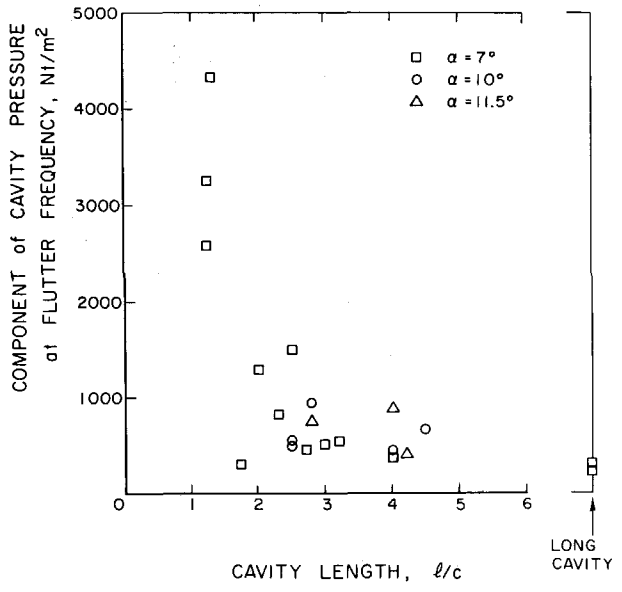

Fig. 8 Magnitude of the fundamental component of the cavity pressure versus the cavity length for all HSWT foils and various angles of attack as indicated

fluence on flutter of the cavity pinch-off and collapse phenomenon described later.

Finally, it is important to record that the foils were also tested in wake flow at tunnel pressures high enough to suppress all cavitation. No sign of flutter could be detected in any of these tests even when the tunnel velocity was much larger than the cavitating flutter speed (see reference [12] for incidental data on the wake pressure fluctuations). It seemed that no dynamic fluid/structure interaction would occur prior to reaching the divergence speed.

Oscillating load displacement and cavity pressure during flutter

The purpose of this section is to record a number of detailed measurements made during the flutter tests in HSWT. Both the leading-edge displacement (from the foil strain gages) and the oscillating load (from the mounting bar strain gage) were recorded during flutter and spectral analysis and cross correlation subsequently performed on a digital signal processor.

Both the displacement and the oscillating load varied with angle of attack and cavity length for a given foil. At the larger angles of attack (10 deg) and greater) the flutter speed was constant with cavity length; hence typical displacement and load amplitudes are plotted against length in Fig. 6. This indicates decreasing amplitudes of flutter with increasing length, a fact referred to previously. On the other hand, at the lower angles of attack (7, 8 deg) the flutter speed changes significantly with cavity length. In this case the variation with flutter speed rather than cavity length is most apparent, and not unexpectedly both amplitudes appear to increase with the square of the velocity as typified by Fig. 7. Furthermore, cross-correlation confirmed that the load (positive upward) was in phase with the foil displacement (positive upward) during flutter.

Measurements were also made of the oscillations in the cavity pressure during flutter; a piezoelectric pressure transducer was mounted within the cavity for this purpose. These measurements indicated that the magnitude of the oscillating cavity pressure was very small (about 400 N·m^2) and its contribution to the oscillating load on the foil was virtually negligible. Though the traces were rather noisy, the basic flutter frequency could be discerned in the signal from the transducer [12]. The magnitudes at the fundamental flutter frequency were obtained by spectral analysis, and all values are plotted together in Fig. 8. They are plotted against cavity length because there appears to be a rough trend for larger oscillating cavity pressures with shorter cavities. No other trends were evident; for example, the cavity pressure oscillations did *not* increase with foil displacement; indeed the reverse seemed to be the case. Cross-correlation of the cavity pressure oscillation and the displacement revealed no consistent relationship, though the cavity pressure generally lagged behind the displacement. All of this suggests that the cavity pressure oscillations play little or no role in the dynamics of flutter and that the cavity pressure remains essentially constant. This is consistent with the fact that the thermodynamic time constant for vaporization is extremely short in water at normal temperatures.

Observations of flow in region of cavity closure

This section is devoted to a description of the interesting events which occurred at cavity closure during flutter. Earlier we remarked on the change in the appearance of cavity closure and cavity wake when flutter occurred; this is illustrated in Fig. 3. Upon closer inspection using high-speed movies taken at 600 frames per second, the following picture emerged. The leading-edge movement during flutter produced a train of waves on the upper cavity surface as sketched in the upper part of Fig. 9. The amplitude of these waves increases as they are convected downstream along the cavity surface. As seen from the cavity interior, the crests become quite sharp and a portion of the cavity is pinched off when a crest reaches the cavity closure region as indicated in Fig. 9. There are some smaller-amplitude waves on the lower surface which play a much lesser role. A detailed frame-by-frame tracing of the pinch-off process is included in Fig. 9. The resulting "separated bubble" had the appearance of a cloud of small bubbles; the interior may however have contained larger voids. It also had the appearance of a pair of cavitated vortices with the upper and lower surfaces rotating in opposite directions. Consequently, the periodic pinching-off also constituted the elements of a Karman vortex street with pairs of vortices imbedded in each separated bubble; clearly this feature is associated with the oscillating lift on the foil. It should be noted that Karman vortex streets in the wake of *steady* cavitating flows have been observed previously [16].

The situation was further complicated by the fact that shortly after pinch-off, these clouds of bubbles collapsed; subsequent rebounds and collapses followed in synchronization with the flutter frequency as the whole structure was convected downstream. A typical volume history for this collapse and rebound process is shown in Fig. 10 for Foil H89 fluttering at a tunnel speed of about 7.9 m/s with a frequency of 60 Hz; the radius of the volumetrically equivalent cylinder for a particular separated bubble is plotted against time. (It should be noted that the significant three-dimensionality could be discerned in the structure after the first rebound.) One should visualize a train of these structures, each separated in time by a flutter period. The time between pinch-off and first collapse varied considerably with different foils and flow configurations and ranged from almost zero up to about 2 flutter periods.

The question arose as to whether the pressure perturbations in the liquid which would be generated by the periodic collapse of the pinched-off bubble clouds could cause sufficient oscillatory loading on the pressure surface of the foil to generate a closed-loop resonant system. One estimate of the magnitude of this radiated pressure perturbation would be $2\rho R(\dot{R})^2/r$ where R and $\dot{R}$ are the radius of the bubble and its time derivative, respectively, and r is the distance to the sensing point (this is based somewhat unrealistically on spherical bubble collapse). Taking typical values of R and $\dot{R}$ from Fig. 10 and the length of the cavity for r, such calculations result in values of the oscillating pressure at the foil which are of the same order of magnitude as those required to cause the

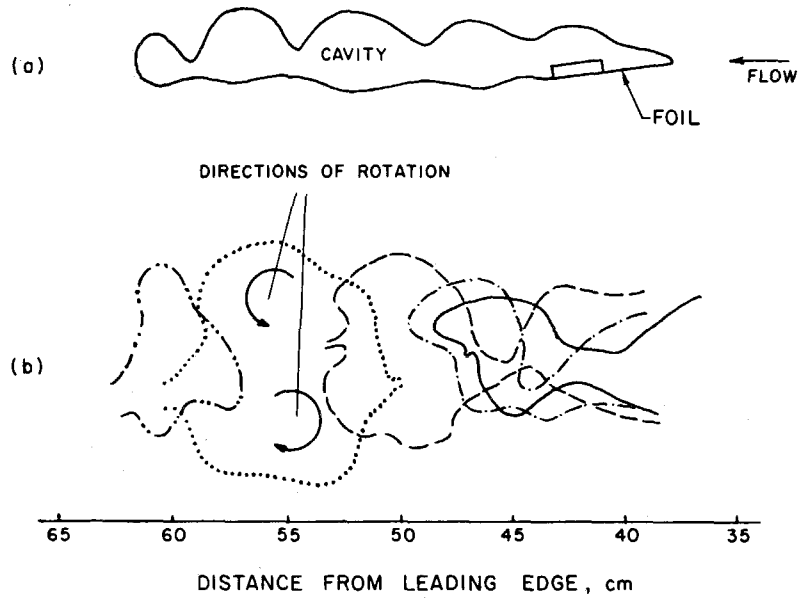

Fig. 9 (*a*) Sketch of the form of the waves on the cavity surfaces during flutter. (*b*) Detailed traces of the pinch-off process in the region of cavity closure. Profiles at the end of the cavity and the pinched-off bubble are shown at times (in seconds) as follows where the origin, $T = 0$, is arbitrary: $T = 0$ ——; $T = 0.005$ –·–; $T = 0.015$ – – –; $T = 0.025$ . . . . . ; $T = 0.055$ — · · — (for Foil H89 at $\alpha = 10$ deg and a velocity of 7.9 m/s). The pinched-off bubble seems to have opposite directions of rotation at the top and bottom as indicated by arrows

observed oscillating lift (about 3000 N·m^2). To examine this further, a piezoelectric pressure transducer was mounted in the tunnel wall to monitor the fluctuating pressure in the water close to the closure region. A typical trace and power spectrum for such measurements is shown in Fig. 11. The harmonic content is consistent with the violent and nonlinear process of cavity collapse. The magnitude of the fundamental component decayed with distance from the closure region as indicated in Fig. 12, and its magnitude was indeed of the order of 3000 N·m^2.

All of this is consistent with the closed-loop resonance mentioned in the preceding. Furthermore, cross-correlations revealed that the pressure perturbations and the foil displacement could either be in-phase with one another or 180 deg out of phase. Any lightly damped system would yield similar results since the phase shift through resonance is very abrupt and one is unlikely to detect the theoretical 90-deg phase shift. Furthermore, it could explain why the flutter speed decreased with decreasing cavity length since the pressure perturbations encountered by the foil are greater for shorter cavities.

Despite all this, the foregoing does not constitute proof that the postulated mechanism is the primary reason for flutter. It will be shown in the next section that leading-edge flutter for cavitating hydrofoils can be explained without any reference to these closure region events. Nevertheless, there seems little doubt that the phenomenon is in some way affected by the closure phenomena. The effect of cavity length and the resonant-length phenomenon are probably outward manifestations of this influence.

Some supplementary data from the FSWT tests

The preliminary experiments in the FSWT were performed prior to those described in the preceding. The detailed results

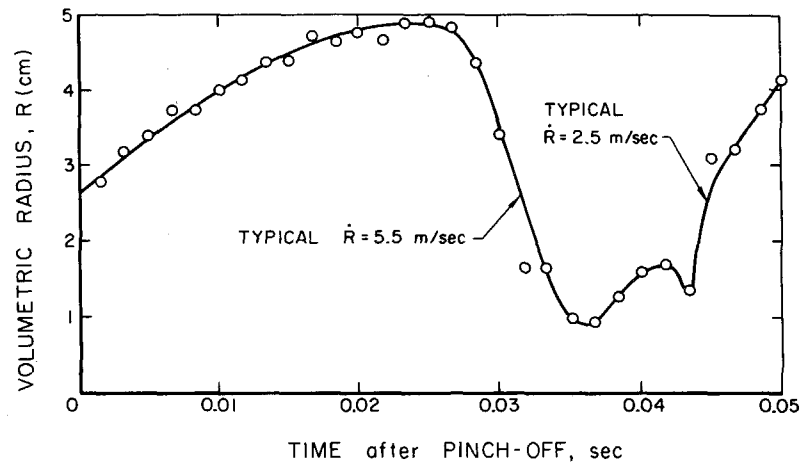

Fig. 10 Volume history of the pinched-off bubble versus time from pinch-off, showing the first collapse and rebound (Foil H89, $\alpha = 10$ deg, $U_F \cong 7.9$ m/s, flutter frequency = 60 Hz)

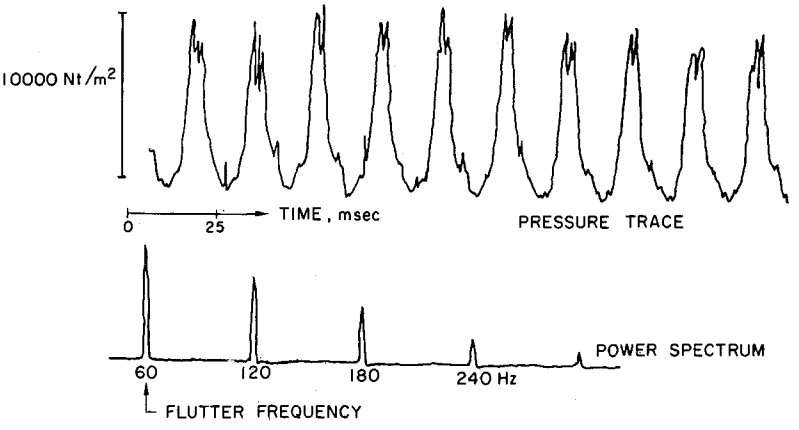

Fig. 11 Typical trace of the pressure in the flow near cavity closure with its power spectrum (Foil H89, α = 7 deg, velocity = 8 m/s, at a point 30 cm downstream of cavity closure)

were not included here for the sake of brevity; they are available in reference [12]. However, several features do deserve brief mention insofar as they contrast or supplement the results from the HSWT tests.

The FSWT tests were conducted with ventilated or air-filled cavities rather than the natural or vapor-filled cavities of the HSWT tests. The air was either supplied artificially to the suction surface of the foils or entered the cavity naturally by ventilation to atmosphere via the wakes of the surface-piercing support struts. Furthermore, the foils listed in Table 2 had a larger, 35.6-cm span and provision was made for external excitation by means of the system described earlier.

The thinnest foil (F16) diverged at a speed lower than that at which a cavity could be generated and F31 exhibited unbounded flutter as soon as a cavity could be formed. The two thicker foils (F61 and F89) both exhibited flutter with ventilated cavities. Perhaps due to the presence of the air in the cavity, the onset was nowhere near as distinct as the onset of flutter in the HSWT tests; indeed the tunnel velocity could be raised significantly higher than the flutter velocity with only a gradual increase in leading-edge amplitude. Furthermore, the reduced flutter velocities for long cavities, though less clearly defined, were significantly lower (about 0.11; see Table 2) than in the HSWT tests. As in the HSWT tests, a minimum flutter speed was observed to occur at an angle of attack of about 10 deg. Steady-state performance measurements revealed no significant change in the steady-state life slope until angles of attack of nearly 20 deg.

Questions concerning the effect of the shape or finish of the leading edges of the foils were also investigated by placing two different shapes of rounded plastic cover over the leading edge of one foil. No significant differences in the flutter behavior were observed with either type of cover despite the fact the separation point was observed to oscillate back and forth on the rounded cover.

Forced-excitation experiments were performed to obtain Q-factors for the foils at velocities up to and beyond the flutter onset speed. The results indicated the expected loss of damping. Furthermore, the resonant frequencies for the foils with ventilated cavities varied only slightly as the tunnel velocity was increased and virtually coincided with the observed flutter frequency (see Fig. 13). These frequencies were surprisingly little different from the natural frequencies in "still" water (see Table 2), considering the fact that one might envisage a substantial decrease in the added mass in a flow with a cavity. This feature was consistent with the HSWT results.

Theoretical analysis

The experimental results indicate that the reduced flutter velocity, $U_F/\omega_F c$, though roughly constant, depends to some extent on the cavitation number (or cavity length), angle of attack, and the mass ratio parameter. In this section we shall explore a simple model for this phenomenon and attempt to collate the observations with previous investigations of conventional flutter for cavitating

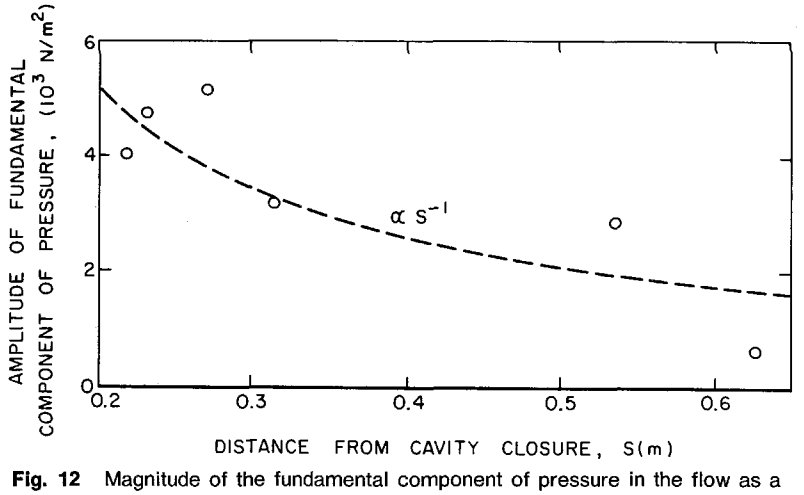

Fig. 12 Magnitude of the fundamental component of pressure in the flow as a function of distance from the cavity closure region

hydrofoils. It can be anticipated, however, that no single model of such a complicated unsteady flow will be capable of explaining all the observed experimental observations.

Perhaps the simplest model is that of a *rigid* foil hinged at some point at or near the training edge; the effective spring constant of the spring which restrains rotational motion about this hinge will be denoted by K. This hypothetical foil (chord, c) can be thought of as performing oscillatory motion identical to that of the zero lift line of the actual foil undergoing leading-edge flutter. The hinge position will be denoted by β where βc is its distance from the leading edge.

Such a model is of course similar to that employed for conventional wing flutter analyses *except* that the possibility of additional heave motion of the hinge point is excluded. The instantaneous angle of attack, α, is subdivided into a mean angle, α_0, and a small time-dependent component, according to

$$\alpha = \alpha_0 + Re\,\{\tilde{\alpha}e^{j\omega T}\} \tag{1}$$

where $\tilde{\alpha}$ represents the magnitude of the oscillations, $\omega = \omega_R + j\omega_I$ is a complex frequency, and T is time. It is convenient to establish the origin of T such that $\tilde{\alpha}$ is purely real. The hydrodynamic moment about the hinge point (positive in the leading-edge-up direction) is similarly represented as

$$M = M_0 + Re\,\{\tilde{M}e^{j\omega T}\} \tag{2}$$

where $\tilde{M} = \tilde{M}_R + j\tilde{M}_I$ is necessarily complex in general. Then if the effective moment of inertia of the foil is I, the equation of the perturbations becomes

$$\tilde{\alpha}(K - \omega^2 I) = \tilde{M} \tag{3}$$

If the coefficient of moment about the hinge point is defined in the conventional manner as $C_M = M/\frac{1}{2}\rho U^2 c^2$, and $\tilde{M}/\tilde{\alpha}$ is replaced by $d\tilde{M}/d\tilde{\alpha}$, the real and imaginary parts of equation (3) yield

$$\frac{1}{2}\rho U^2 c^2 \frac{d\tilde{C}_{MR}}{d\tilde{\alpha}} = K - I(\omega_R^2 - \omega_I^2) \tag{4}$$

$$\frac{1}{2}\rho U^2 c^2 \frac{d\tilde{C}_{MI}}{d\tilde{\alpha}} = -2I\omega_R\omega_I \tag{5}$$

where the quantity $\tilde{C}_M = \tilde{C}_{MR} + j\tilde{C}_{MI}$ will be obtained from the unsteady hydrodynamics and will be a function of the reduced frequency, $k = \omega_R c/U$.

It follows that the divergence speed, U_D (if it exists), is given by

$$U_D^2 = 2K/\rho c^2 \left(\frac{d\tilde{C}_M}{d\tilde{\alpha}}\right)_{k=0} \tag{6}$$

On the other hand, flutter may occur if ω_I is negative for any nonzero value of ω_R; this implies from equation (5) that the system is unstable if $d\tilde{C}_{MI}/d\tilde{\alpha} > 0$ and that the neutral stability or flutter point is given by

$$\left(\frac{d\tilde{C}_{MI}}{d\tilde{\alpha}}\right) = 0 \text{ for } \omega_R \neq 0 \tag{7}$$

This will determine a reduced flutter frequency $k_F = \omega_F c/U_F$.

The flutter speed, U_F, and frequency, ω_F, will then follow from equation (4), which can be written as

$$\frac{d\tilde{C}_{MR}}{d\tilde{\alpha}} = \left(\frac{2K}{\rho c^2}\right)\frac{1}{U^2} - 2I_0\mu k^2 \tag{8}$$

where μ is the mass ratio $\mu = \rho_s t/\rho c$ and I_0 is a dimensionless moment of inertia for the foil ($I = I_0\rho_s t c^3$). At $k = k_F$, this yields $U = U_F$, given $I_0\mu$, $2K/\rho c^2$, and the value of the left-hand side at $k = k_F$.

Consider first the case of subsonic, noncavitating and nonseparating flow examined by Smilg [17] using Theodorsen's linearized unsteady airfoil theory. Smilg found that single-degree-of-freedom flutter could occur only when the hinge was located between the leading edge and the quarter-chord point ($0 < \beta < 0.25$); otherwise $d\tilde{C}_{MI}/d\tilde{\alpha}$ was negative for all nonzero values of k. Even within the range $0 < \beta < 0.25$, single-degree-of-freedom flutter could occur only for foils with very large mass ratios. Consequently, single-degree-of-freedom flutter will not occur for practical foils such as those employed in the present experiments. In the noncavitating tests discussed earlier, however, the flow was clearly separating from the leading edge and forming a wake. It might be suggested that the dynamics under these circumstances would be more akin to those of the cavitating flow as anticipated by Woods [18]. The present tests did not support this view; though the cavitating foils fluttered, there was no evidence of flutter in noncavitating flow at speeds as much as 50 percent greater than the cavitating foil flutter speed. The reason for this discrepancy is not entirely clear but is probably due to the differences in the dynamic response of free shear layers and cavity-free surfaces.

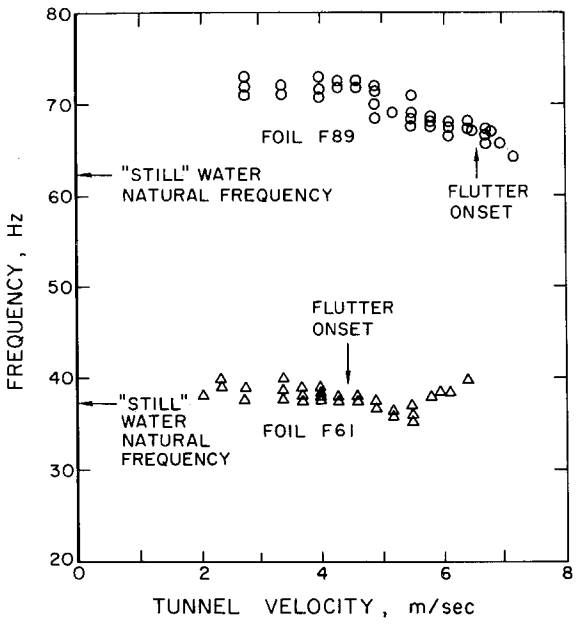

Fig. 13 Natural frequencies for Foils F61 and F89 as a function of tunnel velocity

Turning now to the case of cavitating flow, we shall restrict our theoretical analysis to the simplest case of infinitely long cavities in an unbounded flow. One of the reasons for this restriction is the difficulty involved in finding satisfactory closure models for the cavity in unsteady flow. Certainly none of the available models come close to representing properly the real events we have described occurring in the closure region. The unsteady lift and moment coefficients for the case of infinitely long cavities were evaluated first by Woods [18] and Parkin [19]. Later the linearized theory for small angles of attack was further developed by Martin [20] and Parkin [21]. In addition, Kelly [22] has extended Woods's [18] results to larger angles of attack and finite cavities. For present purposes we shall employ Martin's and Parkin's linearized results which yield a moment coefficient about the hinge point given by

$$\frac{2}{\pi}\frac{dC_M}{d\tilde{\alpha}} = -\frac{5}{16}\left\{\Omega(k) + \frac{5}{8}jk - \frac{245}{512}k^2\right\} + \beta\left\{\Omega(k) + \frac{5}{16}jkW(k) - \frac{35}{64}k^2\right\} - \beta^2\left\{jkW(k) - \frac{9}{16}k^2\right\} \tag{9}$$

where $\Omega(k)$ and $W(k)$ are complex functions tabulated by Parkin [21]. A polar plot is presented in Fig. 14 for various locations of the hinge point, β; values of k are indicated on the curves. Note that in direct contrast to the Smilg case the flow with an infinite cavity *will* exhibit single-degree-of-freedom flutter if the effective

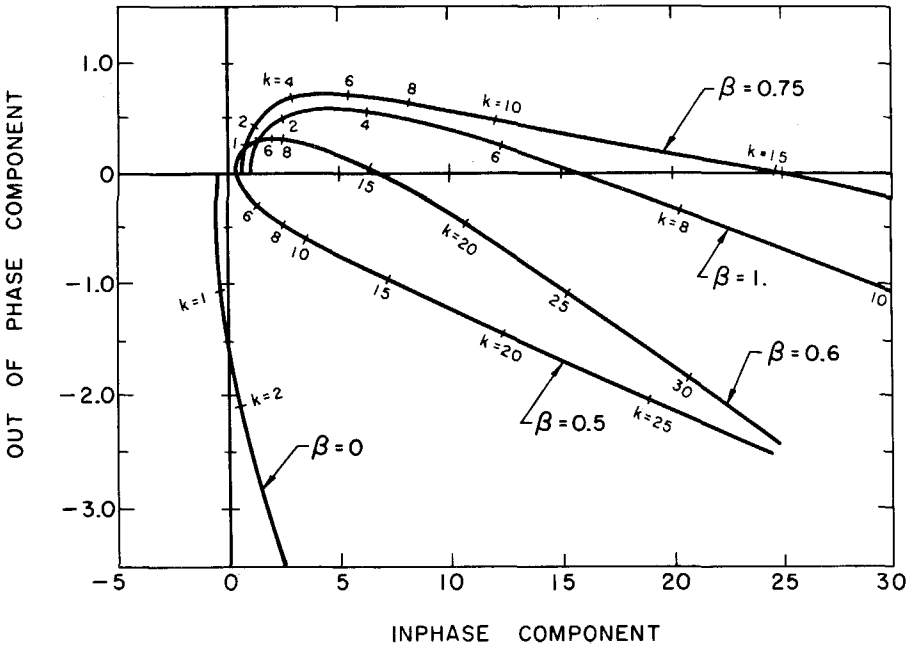

Fig. 14 A polar plot of $(d\tilde{C}_{MI}/d\tilde{\alpha})$ versus $(d\tilde{C}_{MR}/d\tilde{\alpha})$ from equation (9) for various locations of the hinge; values of the reduced frequency, k, are indicated at various points along the curves

hinge point is anywhere between about midchord and the trailing edge ($\beta = 1$). The critical or flutter-reduced frequency, k_F, for which $d\tilde{C}_{MI}/d\tilde{\alpha} = 0$, is plotted against the hinge position, β, in Fig. 15; also shown is the corresponding value of $d\tilde{C}_{MR}/d\tilde{\alpha}$ at $k = k_F$. It remains to determine whether single-degree-of-freedom flutter or divergence will occur by comparing the flutter speed, U_F, with the divergence speed, U_D. From equations (6) and (8) it is clear that

$$\frac{U_F^2}{U_D^2} = \left(\frac{dC_{MR}}{d\tilde{\alpha}}\right)_{k=0} \Big/ \left[\left(\frac{dC_{MR}}{d\tilde{\alpha}}\right)_{k=k_F} + 2I_0\mu k_F^2\right] \tag{10}$$

From expression (9)

$$\left(\frac{d\tilde{C}_{MR}}{d\tilde{\alpha}}\right)_{k=0} = \frac{\pi}{2}\left(\beta - \frac{5}{16}\right) \tag{11}$$

and this is included in Fig. 15. Consequently, the flutter speed is virtually always less than the divergence speed, irrespective of $I_0\mu$. Indeed the foil will exhibit single-degree-of-freedom flutter at speeds far below the divergence speed as demonstrated by the values of U_F/U_D plotted in Fig. 16 for various hinge point locations and values of $I_0\mu$. Furthermore, the flutter frequency, ω_F, is

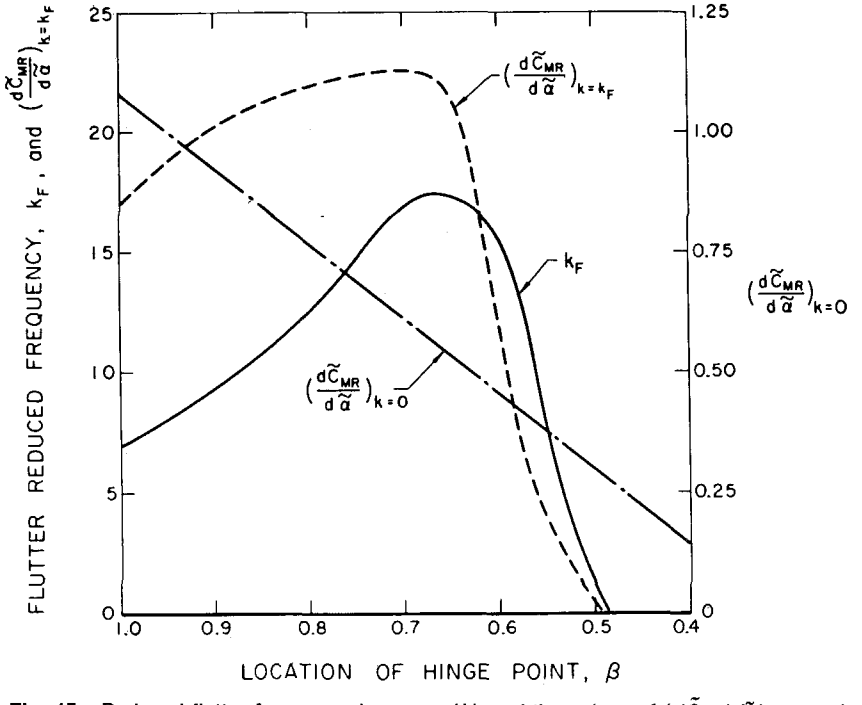

Fig. 15 Reduced flutter frequency $k_F = \omega_F c/U_F$ and the values of $(d\tilde{C}_{MR}/d\tilde{\alpha})_{k=k_F}$ and $(d\tilde{C}_{MR}/d\tilde{\alpha})_{k=0}$ as functions of the hinge location

readily related to the natural frequency of the foil in a flow at speeds much smaller than the flutter speed (denoted by ω_N) by

$$\frac{\omega_F}{\omega_N} = \left[\left\{\left(\frac{1}{k^2}\frac{d\tilde{C}_{MR}}{d\tilde{\alpha}}\right)_{k\to\infty} + 2I_0\mu\right\} \Big/ \left\{\left(\frac{1}{k^2}\frac{d\tilde{C}_{MR}}{d\tilde{\alpha}}\right)_{k=k_F} + 2I_0\mu\right\}\right]^{1/2} \quad (12)$$

As seen by the plots included in Fig. 16, ω_F/ω_N for small values of $I_0\mu$ is virtually always between 0.85 and 0.9 and tends toward 1.0 for very large $I_0\mu$.

It is surprising that this unique feature of supercavitating foil dynamics has received little attention in previous studies, despite the fact that it was briefly alluded to by Woods [18] in his pioneering calculations of the unsteady lift and moment coefficients. What makes it more surprising is the fact that most supercavitating foils with wedge-like thickness distributions will have an elastic axis at a distance about $2c/3$ from the leading edge and hence *will* be susceptible to single-degree-of-freedom flutter. Kaplan and Henry [5] and Song [6] both performed conventional two-degree-of-freedom wing flutter analyses for supercavitating hydrofoils without mentioning the simpler instability. The experiments of Kaplan and Lehman [8], Song and Almo [7], and Cieslowski and Pattison [23] all utilized systems with elastic axes *forward of midchord* and are therefore relevant only to the possibility of the conventional wing flutter which could arise under these circumstances. We have not been able to identify any other experimental results for the more practical supercavitating foil case in which the elastic axis is aft of midchord.

Discussion and conclusions

The experimental reduced flutter speeds for long cavities (see Fig. 4) are in the range 0.15 to 0.25, corresponding to a range of reduced frequencies, k_F, from 7 to 4. These are in fair agreement with the theoretical results for a model hinged at the trailing edge for which $k_F = 7$. One might argue that it is more appropriate to use a theoretical model whose chord is equal to the flexible chord, a, in the experiments. However, this yields theoretical k_F values of about 12 which are even further from the $4 \to 7$ range observed experimentally. It should be appreciated, however, that the model is rather crude and that the oscillatory camber which is absent in the model may have significant dynamic effects. Recently Murai [24] and Shimuzu [25] have computed reduced flutter frequencies for various shapes of foils rigidly supported at their trailing edge. Their value of $k_F = 12$ for a flat plate suggests that the oscillating camber has neither a large nor an unexpected effect.

The experimental observation of a minimum flutter speed at an angle of attack of about 10 deg cannot, of course, be predicted by a linear theory whose results are independent of α_0. It is interesting to note that Kelly's [22] nonlinear calculations at $\alpha_0 = 0$, 10, 20, and 30 deg reveal some instances in which the coefficients exhibit extremums at 10 deg. However, more pertinent evaluation of polar plots like those of Fig. 14 using Kelly's tables indicated that though the values of $d\tilde{C}_{MI}/d\tilde{\alpha}$ increased considerably with α_0, neither the value of k_F nor the value of $(d\tilde{C}_{MR}/d\tilde{\alpha})_{k=k_F}$ was substantially different from those given in Fig. 15.

Kelly's results can also be used to assess the effect of cavity length since he calculated coefficients for cavitation numbers greater than zero (0.3, 0.6, and 0.9). In general the shorter cavities yield marginally smaller values for k_F. Superficially this is consistent with the experimental trend. We believe, however, that the cavity closure dynamics discussed earlier cause substantial alterations in the flutter dynamics for short cavities. None of the theoretical models adequately incorporates these observed closure phenomena.

Some other interesting trends emerge from a comparison of experimentally measured lift and moment coefficients with those

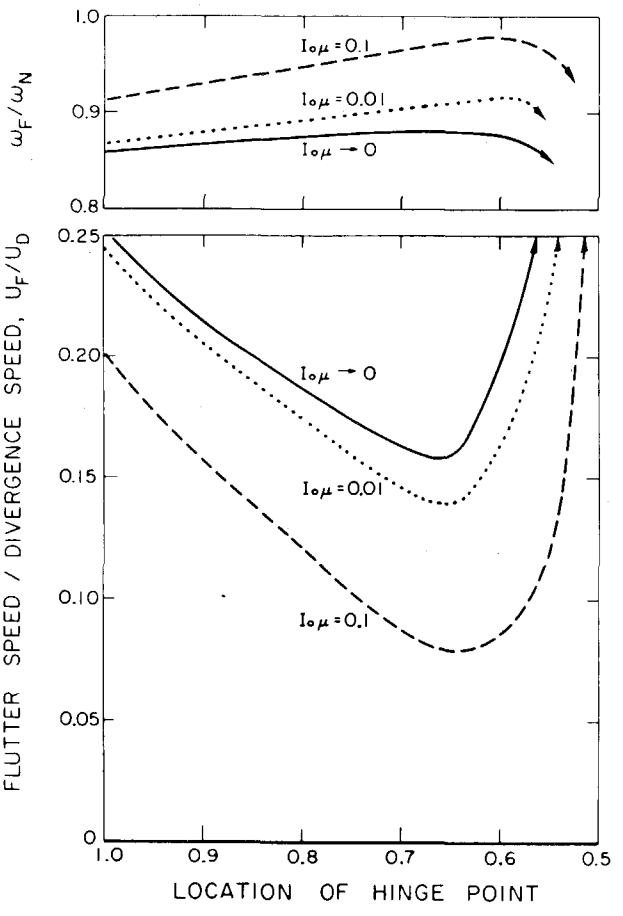

Fig. 16 Values of the ratio of flutter speed to hypothetical divergence speed, U_F/U_D, and the ratio of flutter frequency to natural frequency in flows at much lower speeds, ω_F/ω_N, as functions of the hinge location for various values of $I_0\mu$

predicted by the theory. DeLong and Acosta [26] measured coefficients for supercavitating hydrofoils performing heave motions only and found that both in phase and quadrature lift coefficients (which would contribute to $d\tilde{C}_{MR}/d\tilde{\alpha}$ and $d\tilde{C}_{MI}/d\tilde{\alpha}$ in our notation) were both in general less than the theoretical values. One could conclude that the resulting experimental k_F would be less than the theory, which is consistent with the results of this investigation. Furthermore Klose and Acosta [27] found that ventilated, air-filled cavities exhibited significant cavity pressure variations. This could account for the fact that their measured in-phase lift coefficients were much larger than the theory and their quadrature coefficients were comparable with the theory. Comparison with DeLong and Acosta's results suggests significant differences between the coefficients for ventilated and natural cavities. In the present tests the air-filled cavities examined in the FSWT tests manifest substantially lower reduced flutter velocities (about 0.11) than the natural cavities in the HSWT tests.

It was also shown in Fig. 16 that the theoretical flutter frequency, ω_F, should be only slightly smaller than the natural frequency, ω_N, in flows with velocity well below the flutter velocity. This was borne out by the experimental results of Fig. 13, which suggest a flutter frequency no more than 10 percent less than ω_N. Furthermore, the experiments indicated that ω_N was close to the natural frequency of the foils in "still" water ω_W (see Tables 1 and 2). This quantity ω_W may be difficult to estimate theoretically, however, as discussed earlier.

Finally, it is necessary to discuss the nature of leading-edge

flutter as defined in the Introduction. It should now be clear that a practical supercavitating foil rigidly supported at one end with its elastic axis aft of the midchord and with a slender leading edge is susceptible to several different instabilities. One can for example identify a simple torsional instability for which the results of the last section are directly applicable. There is also the possibility of leading-edge flutter which involves chordwise bending and large amplitudes at the slender leading edge. The flutter speed for each of these will presumably be governed by $U_F^* = \omega_F^* c^*/k_F^*$ where ω_F^* is the natural underwater frequency in that mode, c^* is an "effective" chord length ($c^* = c$ for torsional instability but less for leading-edge flutter), and k_F^* is the appropriate critical constant for each instability. Now ω_F^* would normally be greater for the leading-edge flutter mode than for torsional instability. However, c^* is less for the former; consequently, it is not immediately obvious which instability will have the lower flutter speed. In this respect it is of interest to review the two cases [3, 4] mentioned in the Introduction. According to Fig. 15, the lowest torsional flutter speed is given by $k_F = 17$. If the cavity surface waves are converted at U_F^*, then this leads to a cavity surface wavelength-to-chord ratio of $\lambda/c = 0.3$. On the other hand, if we estimate leading-edge flutter to occur when $\omega_F^* c^*/U_F \approx 3(c^* \equiv a$ = effective flexible chord), then $\lambda/c^* \cong 2$. Now the photographs of Waid and Lindberg [3] and Spangler [4] indicate c/λ-values of about 4 and 8, respectively. This suggests that leading-edge flutter was predominant in both cases with effective flexible chord lengths of $c/8$ and $c/16$, respectively.

The present report has concentrated on a fundamental investigation of leading-edge flutter and has demonstrated conclusively the existence of the phenomenon. The experimental models were designed to have relatively simple modes of vibration and it has been demonstrated that once these underwater modes and natural frequencies are known, reasonable estimates can be made of the leading-edge flutter speed. Furthermore, a rather simple theoretical model yields values of the critical reduced velocity, $1/k_F$, which are within a factor of two of the observations and could be used as conservative design estimates since they are lower than those observed experimentally.

Acknowledgments

The authors are very grateful to a number of people whose help and guidance was invaluable. Discussions with A. J. Acosta and T. Y. Wu were greatly appreciated. Help given by T. Ward, J. Kingan, H. Gabler, H. Hamaguchi, V. Sodha, and C. Hemphill is gratefully acknowledged. Finally, we are most appreciative of the support provided by the General Hydrodynamics Research Program of the David W. Taylor Naval Research and Development Center under Contract No. N00014-75-C-0379.

References

1 Abramson, H. N., "Hydroelasticity: A Review of Hydrofoil Flutter," *Applied Mechanics Reviews*, Vol. 22, No. 2, 1969, pp. 115–121.

2 Acosta, A. J., "Cavity and Wake Flows," *Annual Reviews of Fluid Mechanics*, Vol. 4, 1973, pp. 243–284.

3 Waid, R. L. and Lindberg, L. M., "Experimental and Theoretical Investigations of a Supercavitating Hydrofoil," California Institute of Technology Engineering Report No. 47-8, April 1957.

4 Spangler, P. K., "Performance and Correlation Studies of BuShips Parent Hydrofoil at Speeds from 40 to 75 Knots," Naval Ship Research and Development Center Report No. 2353, 1966.

5 Kaplan, P. and Henry, C. J., "A Study of the Hydroelastic Instabilities of Supercavitating Hydrofoils," JOURNAL OF SHIP RESEARCH, Vol. 4, No. 3, Dec. 1960, pp. 28–38.

6 Song, C. S., "Flutter of Supercavitating Hydrofoils—Comparison of Theory and Experiment," JOURNAL OF SHIP RESEARCH, Vol. 16, No. 3, Sept. 1972, pp. 153–166.

7 Song, C. S. and Almo, J., "An Experimental Study of the Hydroelastic Instability of Supercavitating Hydrofoils," St. Anthony Falls Hydraulic Laboratory Project Report No. 89, University of Minnesota, Minneapolis, Minnesota, 1967.

8 Kaplan, P. and Lehman, A. F., "An Experimental Study of Hydroelastic Instabilities of Finite Span Hydrofoils Under Cavitating Conditions," *AIAA Journal of Aircraft*, Vol. 3, No. 3, 1966, pp. 262–269.

9 Ward, T. M., "The Hydrodynamics Laboratory at the California Institute of Technology—1976," *Trans. ASME, Journal of Fluids Engineering*, Vol. 98, Series 1, No. 4, 1976, pp. 740–748.

10 Ward, T. M., "Report on Water Tunnel Test of Three Hydrofoils Having Very Sharp Leading Edges in Fully Wetted and Cavitating Flows," Galcit Report, HSWT-1124, California Institute of Technology, Pasadena, California, 1976.

11 Oey, K. T., "Leading Edge Flutter of Supercavitating Hydrofoils," Ph.D. Thesis, California Institute of Technology, Pasadena, California, 1979.

12 Brennen, C., Oey, K. T., and Babcock, C. D., "Leading Edge Flutter of Supercavitating Hydrofoils," California Institute of Technology Engineering Report No. 216.1, Pasadena, California, May 1979.

13 Osterwalder, J. and Sonsino, M., "Investigations Concerning Natural Vibrations and Flow Induced Vibrations on Kaplan Turbine Runner Blades," *Proceedings*, 5th Conference on Fluid Machinery, Budapest, Hungary; Akademioi Kiado, Budapest, 1975.

14 Barton, M. V., "Vibration of Rectangular and Skew Cantilever Plates," *Journal of Applied Mechanics*, Vol. 18, No. 2, 1951, pp. 129–134.

15 Lindholm, U. S., Kana, D. D., Chu, W. H., and Abramson, H. N., "Elastic Vibration Characteristics of Cantilever Plates in Water," JOURNAL OF SHIP RESEARCH, Vol. 9, No. 1, March 1965, pp. 11–36.

16 Young, J. O. and Holl, J. W., "Effects of Cavitation on Periodic Wakes Behind Symmetric Wedges," *ASME Journal of Basic Engineering*, Vol. 88, No. 1, 1966, pp. 163–176.

17 Smilg, B., "The Instability of Pitching Oscillation of an Airfoil in Subsonic Incompressible Potential Flow," *Journal of the Aeronautical Sciences*, Vol. 16, No. 11, 1949, pp. 691–696.

18 Woods, L. C., "Aerodynamic Forces on an Oscillating Aerofoil Fitted with a Spoiler," *Proceedings of the Royal Society*, Series A, Vol. 239, 1957, pp. 328–337.

19 Parkin, B. R., "Fully Cavitating Hydrofoils in Nonsteady Motion," California Institute of Technology Engineering Report No. 85-2, Pasadena, California, 1957.

20 Martin, M., "Unsteady Lift and Moment on a Fully Cavitating Hydrofoil at Zero Cavitation Number," JOURNAL OF SHIP RESEARCH, Vol. 6, No. 1, March 1962, pp. 15–25.

21 Parkin, B. R., "Numerical Data on Hydrofoil Response to Nonsteady Motions at Zero Cavitation Number," JOURNAL OF SHIP RESEARCH, Vol. 6, No. 3, Dec. 1962, pp. 40–42.

22 Kelly, H. R., "An Extension of the Woods Theory for Unsteady Cavity Flows," *ASME Journal of Basic Engineering*, Vol. 89, No. 4, 1967, pp. 798–806.

23 Cieslowski, D. S. and Pattison, J. H., "Unsteady Hydrodynamic Loads and Flutter of Two-Dimensional Hydrofoils," SNAME Hydrofoil Symposium, Paper No. 2-b, 1965; also published as: Cieslowski, D. S., "Flutter of a Two-Dimensional Two-Degree-of-Freedom Hydrofoil," Naval Ship Research and Development Center Test Report No. 051-H-01, Feb. 1965.

24 Murai, H., "Theoretical Study of a Flexible Supercavitating Hydrofoil," Japanese Society of Mechanical Engineering 91st Conference, Paper No. 218, 1978, pp. 211–213 (in Japanese).

25 Shimizu, S., Institute of High Speed Mechanics, Tohuku University, Sendai, Japan, personal communication, 1979.

26 DeLong, R. K. and Acosta, A. J., "Experimental Investigation of Non-Steady Forces on Hydrofoils Oscillating in Heave," California Institute of Technology Engineering Division Report, Pasadena, California, March 1969.

27 Klose, G. J. and Acosta, A. J., "Unsteady Force Measurements on Superventilated Hydrofoils in Heaving Motion, JOURNAL OF SHIP RESEARCH, Vol. 13, No. 2, June 1969, pp. 92–102.